Eduvest – Journal of Universal Studies
Volume 6 Number 2, February, 2026
p- ISSN 2775-3735- e-ISSN 2775-3727

Evaluation of Sa210 Grade A1 Steel Degradation Through Hardness and Microstructural Changes After High Temperature Exposure

Yayang Rusdiana[1]*, Rio Pudjidarma Santoso[2], Winarto Winarto[3]
Universitas Indonesia, Indonesia
Email: yayang.rusdiana@ui.ac.id* , rio.pudjidarma41@ui.ac.id, winarto@metal.ui.ac.id

ABSTRACT

SA210 Grade A1 steel pipes are ferritic-pearlitic steels which are commonly used in subcritical boilers. This study investigates degradation characteristics material of SA210 Grade A1 boiler steel under high-temperature operating conditions. The research examines the relationship between microstructural grain size and material hardness under control spheroidization heat treatment (SHT) with time and temperature as parameters. The virgin specimens of SA210 Grade A1 were subjected to temperatures of 600 °C, 660 °C, and 720 °C for durations ranging from 1 h to 100 h, followed by microstructural observation using optical microscopy and Vickers microhardness testing in accordance with ASTM E112 and ASTM E384-17 standards. The findings reveal that higher temperatures and longer exposure times promote pearlite spheroidization and grain size growth, which result in progressive hardness value of the material SA210 Grade A1. The hardness decreased from 167.87 HV in the virgin condition to 121.80 HV at the highest SHT parameter (720 °C – 30 h), corresponding to a 27.4 % reduction. Statistical regression modelling analysis indicated a strong correlation between hardness degradation and material hardness values against thermal exposure at high temperatures. These findings confirm that temperature is the dominant factor initiating grain size coarsening, while exposure duration governs the extent of microstructural degradation. The established correlation provides a simple yet quantitative approach for remaining life assessment of ferritic-pearlitic boiler steels operating under high-temperature service conditions.

KEYWORDS SA210 Grade-A1, Spheroidization, Microstructure, Hardness, Degradation, Boiler Steel

This work is licensed under a Creative Commons Attribution-ShareAlike 4.0 International

INTRODUCTION

SA210 Grade A1 steel pipes are ferritic-pearlitic steels which are commonly used in subcritical boilers. The material is built to operate reliably under demanding conditions including high pressure, elevated high temperatures, and corrosive environments (Pawla et al., 2024). The prolonged use of SA210 Grade A1 steel pipes at elevated temperatures leads to material aging and degradation, characterized by grain structure alterations and a reduction in hardness, which in turn increases the material's susceptibility to deformation under operational pressure (Yu et al., 2024). Corrosion resistance is important parameter, because pipes are often exposed to high temperature to corrosive environments, which can significantly impact their longevity and reliability (Klevtsov et al., 2005). Long-term exposure to excessive heat was identified as the most common cause of boiler failure contributing to 23.4% of all recorded cases (Liu et al., 2022; Wang et al., 2024). Data from coal-fired power plants in Indonesia indicate that tube failures in 315 MW units typically necessitate about five days for repair, with each occurrence resulting in financial losses estimated at approximately IDR 40 billion.

Exposure of SA210 Grade A1 steel to high-temperature environments increases the spheroidization of cementite in the lamellar pearlite structure (Masoumi et al., 2024, 2025). This transformation reduces the pearlite grain fraction and alters the overall grain morphology, becoming a primary factor contributing to the deterioration of the material's

mechanical properties (Li et al., 2020). In the lamellar pearlite structure of the material which consists of alternating layers of ferrite and cementite, thermal instability occurs at elevated temperatures (Li et al., 2020; Sharma et al., 2020). To minimize surface energy and achieve a more stable condition the grains undergo transformation into a spherical morphology. Spheroidization and the segregation of alloying elements in steel result in a more refined microstructure which in turn diminishes the materials mechanical strength (Tokaji et al., 1988). Spheroidization and the segregation of alloying elements in steel lead to softening and reducing the material's resistance to plastic deformation and resulting in a decline in strength. This loss of strength may contribute to crack initiation which can eventually lead to fracture. The spheroidal morphology within the microstructure along with the remaining pearlite fraction and serves as a significant indicator for evaluating the structural integrity of the steel (Adachi & Wang, 2018; Levitin, 1980).

Material condition is usually evaluated when the equipment is not operating (for example during scheduled maintenance), by collecting data and analyzing it to determine the level of damage or suitability of the material. The primary objective is to identify critical areas that may be susceptible to damage. Non-destructive testing (NDT) methods such as metallographic examinations, hardness measurements value and deformation analysis, are commonly employed as preliminary tools to evaluate the material's condition (Akbar et al., 2023), although they have inherent limitations in accurately estimating the remaining safe operating life. There is still limited understanding of the deterioration in mechanical performance and the metallurgical evolution of SA210 Grade A1 steel under long-term aging in actual boiler service conditions. Although the data obtained are essential for evaluating the actual condition of the material, they are not yet widely or systematically integrated into predictive life assessment models (Nasiri & Mirzadeh, 2019).

This research was conducted to study how the properties and conditions of materials change due to high temperatures, with the aim of understanding more deeply the damage (degradation) process that occurs in SA210 Grade A1 boiler steel pipes during use. At each stage of spheroidization degradation of the microstructure was analyzed to detect and clarify the progression of grain size evolution and its effect on changes in hardness. The findings are expected to serve as valuable reference for the monitoring and inspection of boiler systems in the industries.

METHOD

This section presents an overview of the SA210 Grade A1, along with the methods used in the study, including spheroidization heat treatment, optical microscopy, and hardness testing (Qi et al., 2023; Vander Voort, 2000). A microstructure degradation classification system as an approach to remaining service life approach is also introduced in this section (Zhao et al., 2016; Harisha et al., 2018). The results of the chemical analysis of the material sample by a Hitachi PMI-MASTER Optical Emission Spectrometer (OES) are summarized in Table 1 (Laqua, 1977). The chemical compositions analysis process of the SA210 Grade A1 steel tube sample is conducted in accordance with ASTM Handbook of Comparative World Steel Standards (ASTM International, 2023).

Table 1. Chemical composition of SA210 Grade A1(%)

	Fe	C	Mn	Si	P	S	Cr	Mo
Standard	Balance	0.27	0.93	0.10 min	≤0.035	≤0.035		
Samples	98.35	0.23	0.78	0.14	0.009	0.006	0.13	0.03

1. Optical Microscopy

Classification system offers a structured framework for assessing microstructural degradation in ferrite-pearlite steel of boiler tube specimens (Dobrzański et al., 2011). This system outlines six distinct morphological stages of pearlite transformation, labeled A through F (Zhao et al., 2016; Toft & Marsden, 1961). Stage A is characterized as a virgin material with intact lamellar structures, which gradually transition into initial spheroidization in Stage B, followed by increasing carbide rounding in Stages C and D. In the final stages, E and F, the microstructure undergoes significant reorganization, marked by the carbide coalescence (Li et al., 2019; Pandit & Bhadeshia, 2012; Dlouhý et al., 2014). Detailed descriptions of each stage are provided in Table 2 (Toft & Marsden, 1961). Microstructural analysis was conducted using an Olympus DSX500 optical microscope at 1000x magnifications, ensured consistent and reliable evaluation of all samples (Mahamood & Akinlabi, 2017).

Table 2. Qualitative characterization of spheroidization on ferrite-pearlite steel

Stage	Remaining life	Description
A	100%	A typical structure of virgin material, where the pearlite (or bainite) regions are clearly visible. The carbides within the pearlite are not entirely lamellar, some gray areas can also be observed
B	80%	Initial breakdown of pearlite lamellae, typically accompanied by the formation of small carbide particles along the grain boundaries. The pearlite structure remains relatively dense and retains much of its original morphology.
C	60%	Clearer indications of the carbide spheroidization in the pearlite regions, although some carbide plates are still present. There is increased carbide precipitation within ferrite grains and along the grain boundaries. The overall morphology of the region remains preserved.
D	40%	Carbide spheroidization is nearly complete, although the particles remain clustered in the original pearlite arrangement.
E	20%	Spheroidization is fully achieved, with carbides uniformly distributed and scanty remnants of the original pearlite structure. However, slight indications of the former pearlite regions can still be detected.
F	End of life	A significant growth in the size of certain carbide particles is observed, partly because of coalescence, with the particles distributed along the ferrite grain boundaries. The original morphology has nearly vanished.

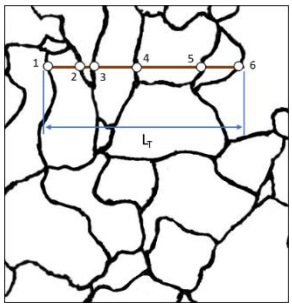

Figure 1. Lineal intercept procedure for grain size measurement according to ASTM E112

Microstructural analysis was performed using ImageJ software. Based on the ASTM E112 standard, which is a guideline for measuring the average grain size, this study uses the intercept method, which is a simple way to calculate the grain size of a material from photographs obtained under an optical microscope (Marcomini & de Souza, 2011; Cui et al., 2022). The intercept method is considered a suitable choice when grain boundaries or interfaces are difficult to distinguish clearly, as it helps minimize significant measurement errors (ASTM International, 2013). This method employs the use of test lines that traverse the microstructural micrograph in a random manner which enables relatively rapid microstructural characterization and can be applied across a wide range of metals and alloys.

As illustrated in Figure 1, the intercept method involves overlaying random test lines on microstructural images and counting the number of intersections between these patterns and the grain boundaries (ASTM International, 2021; ISO, 2019; JIS, 2020; GB/T, 2017). In the intercept method, a random test pattern in the form of a line or circle is drawn on the microscope image, then the number of intersection points (NL) between the pattern and the grain boundaries is counted. The grain size number (G), which is a common index for evaluating grain size based on the number of intersections can be determined using the Eq. (1) (Cui et al., 2022).

$$G = -6.643856 \times log_{10}\ell - 3.288 \quad (1)$$

$$\ell = \frac{L}{M \times N_L} \quad (2)$$

Where l is the mean intercept length (mm), L is the total length of test patterns (mm), and NL is the number of intersections. Since the L and M values generally remain constant in the evaluation of the same set of microstructural images, the accuracy in calculating the number of intersections becomes the most crucial aspect in applying the intercept method [32].

2. Spheroidization Heat Treatment

The degradation mechanism of SA210 Grade A1 steel was examined using an accelerated aging approach in combination with several characterization methods. According to earlier study of Salonen and Auerkari on St35.8 steel, which equivalent to SA210 Grade A1, this study employed a controlled spheroidization heat treatment (SHT) to replicate the effects of long-term thermal exposure within a shortened laboratory timeframe (Salonen & Auerkari, 1996; Qi et al., 2023). Virgin SA210 Grade A1 specimens were exposed to carefully regulated thermal cycles with a heating rate of 300°C per hour until target temperatures of 600°C, 660°C, or 720°C were reached (Toft & Marsden, 1961). This temperature is then maintained for 1 to 100 hours to produce varying degrees of microstructural changes due to heating. Following each isothermal holding stage, the specimens were cooled gradually within the furnace to room temperature to avoid thermal shock. The experimental matrix, detailed in Table 3, establishes a systematic link between specific temperature-time conditions and the approximation stages of spheroidization development (Toft & Marsden, 1961).

Table 3. Variation of temperature and aging duration of spheroidization heat treatment [25]

Temperature (^oC)	-	600	660	600	660	600	720	720	660	720
Holding time (hour)	-	3	1	30	3	100	1	3	100	30

Equivalence spheroidization stage	A	B	B	C	C	D	D	D	E	F

3. Hardness Measurement

Hardness testing was performed in accordance with ASTM E384-17 (ASTM International, 2017): Standard Test Method for Microindentation Hardness of Materials. Microhardness testing was conducted using the Vickers (HV) method with a Future Tech FM-810 hardness tester. This hard measurement was carried out at room temperature, applying a 10 kgf load with a pyramidal diamond indenter and a dwell time of 10 seconds. This setup was selected to maintain uniform indentation geometry across all samples and to reduce variability in the measurement results.

RESULT AND DISCUSSION

The Spheroidization heat treatment caused a very significant microstructural transformation in SA210 Grade A1 specimens accompanied by a measurable reduction in hardness. Figure 2. displays the baseline microstructure of virgin material (Stage A) which shows a typical two-phase morphology. Consistent with the classification in Table 2, distinct ferrite matrix regions (light areas) alternate with pearlite colonies (dark regions). Pearlite structure is a microstructure in steel that is formed from the arrangement of cementite and ferrite according to the iron-carbon (Fe–C) phase diagram.

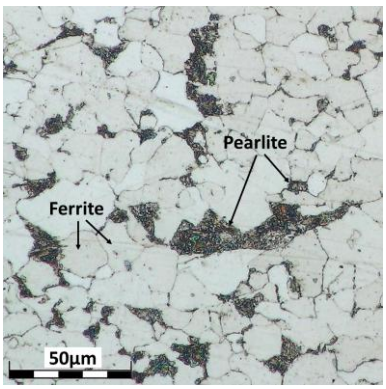

Figure 2. Microstructure of virgin SA210 Grade A1 steel

As shown in Figure 3, the spheroidization heat treatment (SHT) produced clear microstructural transformations, which reflected the specific combinations of temperature and time applied. At stage B after 3 hours at 600 °C and 1 hour at 660 °C, the lamellar pearlite begins to lose its continuity and cementite dissolution is evident (Figure 2a-b). Progressive degradation to Stage C, by 600 °C for 30 hours and 660 °C for 3 hours SHT, pearlite colonies become less distinct as cementite dissolution continues (Figure 2c-d). With longer aging, ferrite grains are more apparent while residual pearlite areas are significantly reduced, indicating advanced carbide dissolution. The morphology reveals spheroidization in progress on Stage D, microstructure shows significant carbide dissolution with pearlite areas becoming less distinguishable (Figure 2e-f). More advanced Stage D, carbides coalesce into discrete globular particles and pearlite lamellae are almost completely replaced by spheroidized

carbides (Figure 2g). At Stage E, continued exposure promotes coalescence and carbides grow larger as they merge, reducing the number of smaller particles (Figure 2h). At the final stage of Stage E, the pearlite structure has practically vanished (Figure 2i). The microstructure SA 210 Grade A1 is dominated by ferrite with fully spheroidized carbides and reflecting extensive coarsening due to long-term aging.

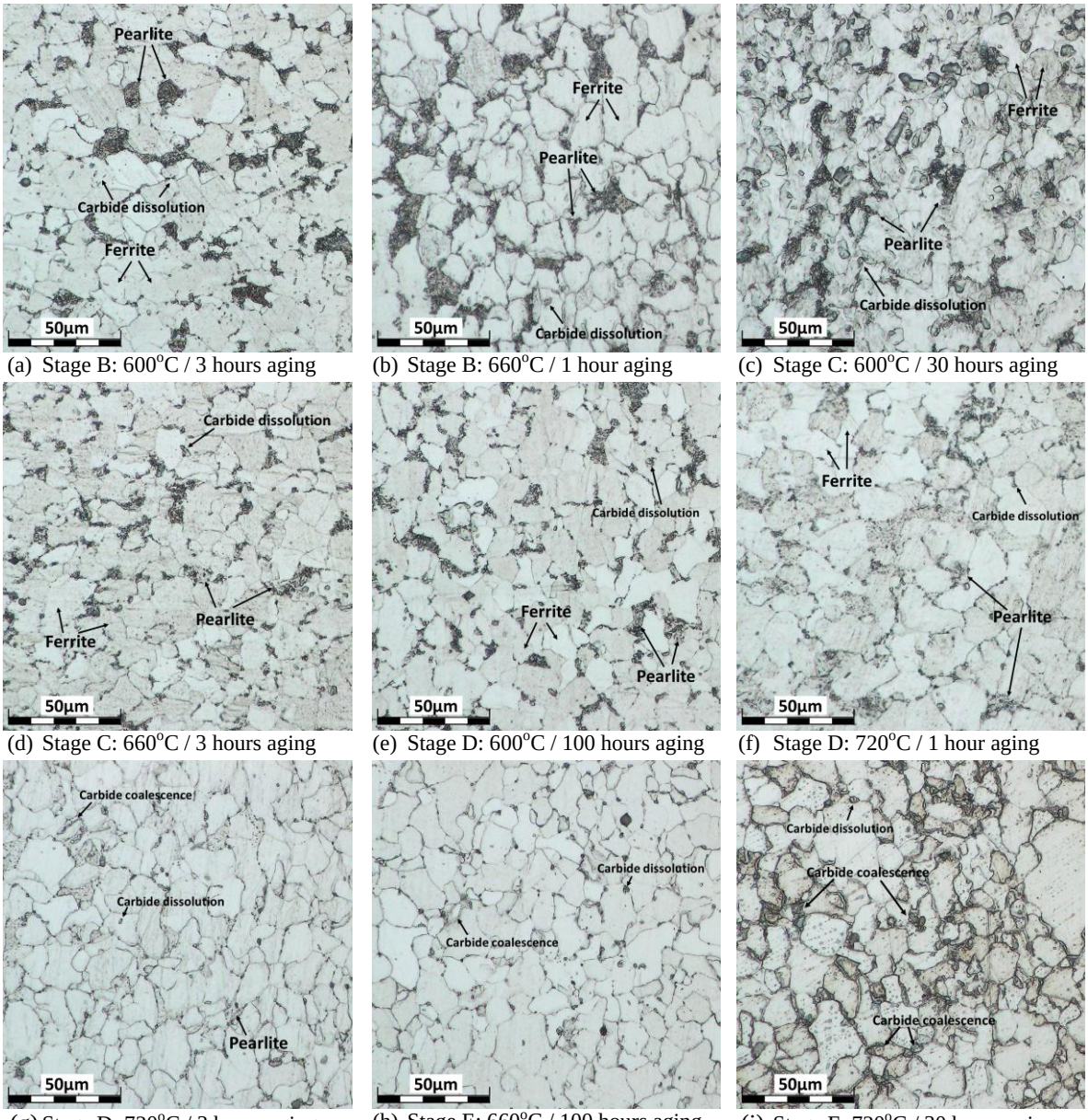

(a) Stage B: 600°C / 3 hours aging (b) Stage B: 660°C / 1 hour aging (c) Stage C: 600°C / 30 hours aging

(d) Stage C: 660°C / 3 hours aging (e) Stage D: 600°C / 100 hours aging (f) Stage D: 720°C / 1 hour aging

(g) Stage D: 720°C / 3 hours aging (h) Stage E: 660°C / 100 hours aging (i) Stage F: 720°C / 30 hours aging

Figure 3. Microstructure degradation evolution after spheroidization heat treatment at different temperature and time

Table 4. Changes in ASTM Grain Size Number (G) under different Spheroidization Heat Treatment parameters

SHT parameters	ASTM Grain Size Number (G)
Virgin material	10.518
600°C – 3 hours	10.377
600°C – 30 hours	10.260

600°C – 100 hours	10.105
660°C – 1 hour	10.348
660°C – 3 hours	10.199
660°C – 100 hours	9.942
720°C – 1 hour	10.073
720°C – 3 hours	10.008
720°C – 30 hours	9.805

The grain size number in this study was determined in accordance with the ASTM E112 intercept method, employing the mathematical relationship on Eq. (1) and (2). To obtain reliable values of l, seven parallel test lines of equal length were superimposed on each micrograph, ensuring consistent sampling across different regions of the microstructure. This approach allows for accurate conversion of values or numbers between the measured intercept length and the actual grain size. Using this standard procedure, the ASTM grain size values obtained reflect the progressive changes in grain size coarsening of the microstructure during heat treatment, thus providing a quantitative basis for correlating grain size evolution with hardness degradation in SA210 Grade A1 steel.

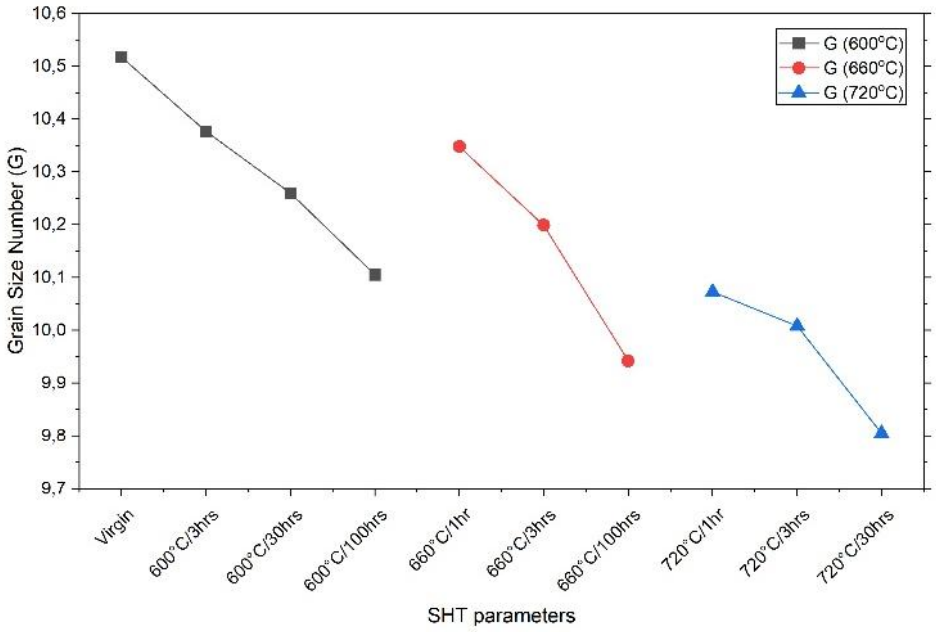

Figure 4 Microstructure degradation evolution after spheroidization heat treatment at different temperature and time

The grain size evaluation of SA210 Grade A1 steel under spheroidization heat treatment revealed a clear dependence on both temperature and holding time on Table 4 and Figure 4. In the virgin condition, the material exhibited a fine microstructure corresponding to an ASTM grain size number of 10.518. Subsequent heating at 600 °C for durations up to 100 hours resulted in only a minor reduction in grain size number, decreasing from 10.377 to 10.105, indicating that grain coarsening was relatively slow at this temperature. At 660 °C, however, a more pronounced decline in grain size number was observed, from 10.348 at 1

hour to 9.942 at 100 hours, demonstrating the onset of accelerated grain growth. The most significant effect occurred at 720 °C, where the grain size number dropped from 10.073 to 9.805 within only 30 hours of exposure, confirming that elevated temperatures substantially promote grain boundary migration and coarsening. Overall, the experimental results show that prolonged exposure to high temperatures causes grain size growth and with the rate of coarsening being strongly influenced by the temperature parameters during the heat treatment.

Table 5. Hardness evolution and spheroidization stages as influenced by SHT parameters

Equivalence spheroidization stage	SHT parameters	Hardness (HV)	Δ Hardness (HV)	Fraction drop (%ΔH)
A	Virgin material	167.87	0	0
B	600°C – 3 hours	151.38	16.50	9.8
B	660°C – 1 hour	150.61	17.26	10.3
C	600°C – 30 hours	146.10	21.77	13.0
C	660°C – 3 hours	144.12	23.75	14.1
D	600°C – 100 hours	140.77	27.10	16.1
D	720°C – 1 hour	139.74	28.13	16.8
D	720°C – 3 hours	131.86	36.01	21.5
E	660°C – 100 hours	125.22	42.65	25.4
F	720°C – 30 hours	121.80	46.07	27.4

A consistent decline in microhardness values, represented here as median values, that correlates with the progressive spheroidization of SA210 Grade A1 specimens is presented in Table 5 and Figure 5. The as-received material (Stage A) recorded an initial hardness of 167.87 HV, representing its undegraded state. A noticeable decrease was observed in Stage B, with reductions of approximately 9.8–10.3%, as indicated by values of 151.38 HV for the 600 °C-3 h SHT parameters and 150.61 HV for the 660 °C-1 h SHT parameters. This stage corresponds to the onset of the spheroidization phenomenon [13]. Further reductions were evident in Stage C, where the hardness decreased to 146.10 HV (600 °C/30 h) and 144.12 HV (660 °C-3 h), equivalent to a 13.0–14.1% drop, indicating partial spheroidization of lamellar carbides. Stage D showed more advanced changes, with values of 140.77 HV (600 °C-100 h, 16.1%), 139.74 HV (720 °C-1 h, 16.8%), and 131.86 HV (720 °C-3 h, 21.5%), reflecting near-complete transformation. Prolonged exposure at 660 °C-100 h led to Stage E characteristics, with a hardness of 125.22 HV (25.4% decrease). Finally, Stage F exhibited the most pronounced degradation, with hardness declining to 121.80 HV (27.4% reduction at 720 °C-30 h), confirming carbide coalescence and microstructural stabilization associated with end-of-life conditions.

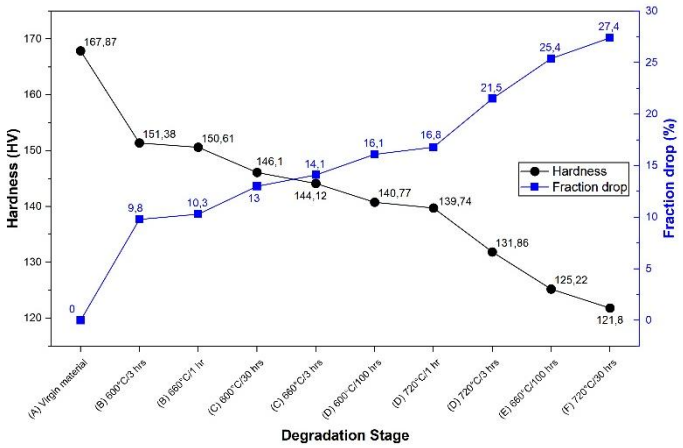

Figure 5. Graphical plot of hardness changes and the degradation stages of spheroidization

To statistically assess the effect of thermal exposure on material hardness degradation, an ANOVA analysis was conducted using the experimental dataset on Table 5. In this dataset, we take X1 which represents the exposure temperature, X2 corresponds to holding time at specified temperature, and Y denotes the resulting percentage in hardness fraction drop. From the regression output on Table 6, the Multiple R value of 0.907 already suggests that the response of hard degradation is tightly linked to the imposed thermal parameters. In practical terms, this means the material reacts quite predictably to temperature and exposure duration. The R^2 value, which reaches 0.823, indicates that a significant share of the hardness reduction which 82.3% can be explained directly by these two variables. Interestingly, the Adjusted R^2 remains at 0.764, which implies that both parameters are genuinely influential rather than statistically inflated. This aligns well with the metallurgical mechanism: temperature triggers the breakdown of lamellar pearlite, whereas longer holding time allows spheroidization and carbide coarsening to progress, leading to a gradual decline in mechanical strength.

Table 6. Regression statistic result as influenced by SHT parameters

Multiple R	0,9074
R Square	0,8235
Adjusted R Square	0,7646
Standard Error	3,0721
Observations	9
Significance F	0,0055

Table 6 also shows Significance F value of 0.0055 confirms that the regression model is statistically significant, and the probability that the observed relationship between temperature, holding time, and hardness reduction occurred by random chance is less than 1%. Consequently, the null hypothesis assuming no influence of the predictors on %ΔH can be rejected with confidence, indicating that the model provides meaningful explanatory power for the degradation response.

Table 7 Regression coefficient result as influenced by SHT parameters

	Coefficients	*Standard Error*	*t Stat*	*P-value*	*Lower 95%*	*Upper 95%*

Intercept	-55,1575	15,0495	-3,6651	0,0105	-91,9822	-18,3327
X1 temperature	0,1046	0,0223	4,6942	0,0034	0,0501	0,1591
X2 holding time	0,1095	0,0280	3,9117	0,0079	0,0410	0,1781

The regression coefficient on Table 7 provides additional insight into the contribution of each predictor variable. Both X1 (temperature) and X2 (holding time) the results show positive coefficient values. measured at 0.1046 and 0.1095, respectively. This indicates that an increase in either temperature or holding duration results in a corresponding increase in hardness fraction drop (%ΔH), confirming a direct degradation trend consistent with thermally activated damage mechanisms in steel. For X1 (temperature) the model yields t = 4.69 (p = 0.0034). Using the reported coefficient (0.1046), this corresponds to a standard error of about 0.0223 and a 95% confidence interval approximately [0.0501, 0.1591]. In plain terms, the temperature coefficient is more than four times its standard error and the 95% interval exclude zero, so there is strong statistical evidence that temperature has a positive and non-negligible effect on hardness fraction drop (%ΔH). For X2 (holding time) the model gives t = 3.91 (p = 0.0079). With the coefficient of 0.1095, the standard error is roughly 0.0280 and the 95% confidence interval is about [0.0410, 0.1781]. This shows that holding time is also a statistically significant predictor: its coefficient is nearly four standard errors from zero and its confidence interval likewise excludes zero. And the last, intercept has a negative value (–55.1575) with a p-value of 0.0105, indicating that it is also statistically significant.

The microstructural evolution of SA210 Grade A1 during aging by SHT [33] is clearly illustrated in the sequence of photomicrographs presented in Figure 3 dan Figure 4. Initially the microstructure is dominated by a well-defined pearlitic morphology with alternating ferrite and lamellar cementite arranged in a parallel configuration. As the aging treatment progresses, driven by both increasing temperature and extended holding time the cementite lamellae begin to lose their continuity [12]. At lowest testing temperature (600oC) with a holding time of 3 hours, only limited cardon diffusion occurs, resulting in a minimal change to pearlite morphology. This behavior contrasts sharply with that observed at elevated temperatures of 660oC and 720oC, where temperature exerts a significant influence on atomic diffusion within the material, even under the same holding time. The increase in temperature can enhance the thermal motion of carbon atoms. Primarily due to a substantial rise in the carbon diffusion coefficient, which in turn accelerates the diffusion rate.

Sustaining exposure to elevated temperatures drives the full spheroidization of cementite, followed by carbide growth controlled by Ostwald ripening processes. Ostwald ripening refers to a thermodynamic process in which small particles dissolve and their material diffuse into larger particles, which then grow at the expense of the smaller particles. This transformation leads the microstructure to develop into a more homogenous distribution of rounded carbides within the ferritic matrix, marked by a gradual loss of interface definition as aging advances.

The grain size evaluation of SA210 Grade A1 steel indicates that microstructural coarsening is strongly governed by temperature, with holding time acting as a secondary accelerating factor. In the virgin condition, the steel exhibited a fine ferrite-pearlite structure with ASTM grain size 10.518, which remained relatively stable at 600oC even after

prolonged exposure. It reflects limited grain boundary mobility at this thermal level. A noticeable transition in coarsening kinetics occurred at 660oC, where the reduction in ASTM grain size number suggests the onset of active boundary migration driven by increased diffusional activity. A significant drop in ASTM grain size number occurred at 720oC within a shorter exposure period, which indicated a shift into an advanced degradation regime characterized by substantial grain boundary migration and reduced interfacial energy. From the results of data observations, it is confirmed that temperature is more dominant in triggering grain hardening, while exposure time influences the level of microstructural degradation. This behavior consists of thermally activated spheroidization and creep-softening mechanisms reported in ferritic-pearlitic boiler steels.

The progressive decrease in hardness across stages A to F reflects a clear correlation between thermal exposure parameters and the extent of microstructural degradation in SA210 Grade A1 steel. The modest hardness reduction observed in stages B and C. It suggests that the steel was still in the early phase of spheroidization, where lamellar pearlite begins to destabilize but carbide particles remain partially intact. This gradual decrease in hardness values indicates that dislocation movement becomes less restricted as the interface between ferrite and cementite loses its sharp morphology. The more substantial hardness loss is noted in stage D, which marks a transition toward advanced spheroidization. In the final stages of degradation (E and F), the initial lamellar pearlite structure becomes entirely unrecognizable. It is transitioning to thermodynamically stable but mechanically compromised configurations characterized by over 27% hardness reductions. At this stage, the material approaches its function limit under service conditions, as the reduction in hardness reflects a marked loss in resistance to creep and deformation. These align with the established metallurgical principles that prolonged thermal exposure accelerates carbide coarsening and grain boundary relaxation. In the end, it is ultimately diminishing the structural integrity of boiler tube operating in high temperature environments.

The percentage decrease in Vickers hardness (decrease in hardness fraction) provides a more reliable metric of degradation than absolute hardness values. This normalized approach accounts for inherent material variability caused by fabrication differences and heat treatment variations in the boiler tube manufacturing processes. By correlating specific percentage hardness drops with a defined spheroidization stage, the establishment of a standardized remaining life assessment method results in a consistent interpretation regardless of initial material properties.

Based on the regression coefficients on Table 7, the empirical model describing the hardness fraction drop (%ΔH) as a function of temperature (T) and holding time (t) can be expressed as:

$$\%\Delta H = -55.15 + 0.1046T + 0.1095t \quad (3)$$

This equation 3. Describes the linear degradation trend of material hardness changes where temperature and exposure time contribute positively to the decrease in hardness value In the experimental domain, a gradual increase in any of the test variables results in a measurable increase in the %ΔH of the material, indicating a continuous decrease in the mechanical properties of the material. Meanwhile, the positive slope coefficient on the graph related to temperature and time reflects the degradation properties caused by temperature in SA210 Grade A1 steel. Higher temperatures can accelerate processes driven by atomic

diffusion, while prolonged exposure provides sufficient time for microstructural instabilities to develop. As a result, the material gradually loses resistance to deformation, which is accurately captured by the increasing ΔH values predicted by the model.

CONCLUSION

This study and work have successfully evaluated the SA210 Grade A1 steel degradation after high temperature exposure and developed a simple predictive approach as a methodology for remaining life assessment (RLA). Several key findings are as follows: Temperature acts as the dominant factor promoting faster carbon diffusion, while prolonged exposure accelerates coarsening kinetics. Grain coarsening intensifies with increasing temperature, where 660°C and 720°C promotes active boundary migration and diffusional growth compared to the stable fine grains at 600°C. The gradual evolution from lamellar pearlite (Stage A) to fully spheroidized carbides (Stage F) shows a strong correlation with hardness loss reaching up to 27.4%, which indicates end-of-life conditions. The normalized percentage reduction in Vickers hardness offers a more consistent measure of material degradation by minimizing the effects of variations in steel fabrication. The regression analysis established a linear empirical model which provides a simple yet quantitative indicator for defining degradation stages, supporting reliable remaining life assessment of boiler tube steels.

REFERENCES

Abrams, H. (1971). Grain size measurement by the intercept method. *Metallography*, *4*(1), 59–78. https://doi.org/10.1016/0026-0800(71)90005-X

Adachi, Y., & Wang, Y.-T. (2018). Topology and differential geometry-based 3D characterization of spheroidized pearlite. In *Advanced characterization of thin film solar cells* (pp. 247–268). Wiley-VCH. https://doi.org/10.1002/9781119426813.ch11

Akbar, S., Nursyifaulkhair, D., Nurdiwijayanto, L., Noviyanto, A., & Rochman, N. T. (2023). High-temperature failure of steel boiler tube secondary superheater in a power plant. *Sinergi*, *27*(1), 1. https://doi.org/10.22441/sinergi.2023.1.001

Alcántara Alza, V. (2021). Spheroidizing in steels: Processes, mechanisms, kinetic and microstructure—A review. *IOSR Journal of Mechanical and Civil Engineering*, *18*(3), 63–81. https://doi.org/10.9790/1684-1803036381

ASTM International. (2013). *ASTM E112-13: Standard test methods for determining average grain size*. ASTM International.

ASTM International. (2017). *ASTM E384-17: Standard test method for microindentation hardness of materials*. ASTM International. https://doi.org/10.1520/E0384-17

ASTM International. (2021). *ASTM E112-13(2021): Standard test methods for determining average grain size*. https://www.astm.org/e011213r21.html

ASTM International. (2023). *Specification for general requirements for carbon and low alloy steel tubes*. https://doi.org/10.1520/a0450_a0450m-23

Cui, X., Li, L., Li, J., Chen, Y., Han, W., Shonkwiler, S., & McMains, S. (2022). Automation of intercept method for grain size measurement: A topological skeleton approach. *Materials & Design*, *224*, 111358. https://doi.org/10.1016/j.matdes.2022.111358

Dlouhý, J., Hauserova, D., & Novy, Z. (2014). Shape evolution of cementite during accelerated carbide spheroidisation. *Materials Science Forum*, *782*, 117–122. https://doi.org/10.4028/WWW.SCIENTIFIC.NET/MSF.782.117

Dobrzański, J., Hernas, A., & Moskal, G. (2011). Microstructural degradation in boiler steels: Materials developments, properties and assessment (pp. 222–271). Woodhead Publishing. https://doi.org/10.1533/9780857093806.2.222

GB/T. (2017). *GB/T 6394-2017: Determination of estimating the average grain size of metal*. Standardization Administration of China.

Harisha, S. R., Sharma, S., Kini, U. A., & Shankar, M. C. G. (2018). Study on spheroidization and related heat treatments of medium carbon alloy steels. *MATEC Web of Conferences*, *144*, 02008. https://doi.org/10.1051/MATECCONF/201814402008

Hu, Y., Shi, Y., Zhang, Y., Jiang, Y., & Wang, J. (2025). Revealing the microstructure evolution and excellent ductility of near-α Ti–6Al–3Nb–2Zr–1Mo alloy via spark plasma sintering using pre-alloyed spherical powders. *Journal of Materials Research and Technology*, *35*, 6247–6260. https://doi.org/10.1016/j.jmrt.2025.02.255

ISO. (2019). *ISO 643:2019: Steels—Micrographic determination of the apparent grain size*. International Organization for Standardization. https://www.iso.org/standard/72193.html

JIS. (2020). *JIS G 0551:2020: Steels—Micrographic determination of the apparent grain size*. Japanese Standards Association.

Klevtsov, I., Tallermo, H., Bojarinova, T., & Crane, R. A. (2005). High temperature corrosion of boiler steels under chlorine-containing surface deposits. *Journal of Pressure Vessel Technology-Transactions of the ASME*, *127*(2), 106–111. https://doi.org/10.1115/1.1876497

Laqua, K. (1977). Optical emission spectrochemical analysis. *Pure and Applied Chemistry*, *49*(10), 1595–1608. https://doi.org/10.1351/PAC197749101595

Levitin, V. V. (1980). The physical mechanism and the structural model of creep in metals. *Physica Status Solidi (a)*, *62*(2), 557–568. https://doi.org/10.1002/PSSA.2210620225

Li, L., Wang, X., Du, Y., Xu, L., Zhao, L., & Han, Y. (2020). Microstructural aging and property degradation of service-exposed 1Cr–1/2Mo coke drum steel. *Materials Science and Technology*, *36*(18), 1943–1953. https://doi.org/10.1080/02670836.2020.1852665

Li, Z.-X., Li, C., Kim, S. H., & Suh, D.-W. (2019). Influence of initial pearlite morphology on the microstructure evolution during heat treatment of 1.0C–1.5Cr steel. *Metals and Materials International*, *25*(1), 9–17. https://doi.org/10.1007/S12540-018-0171-Y

Liu, G., Yang, X., Yang, X., Liang, K., An, D.-H., & Ren, X. (2022). Typical damage prediction and reliability analysis of superheater tubes in power station boilers based on multisource data analysis. *Energies*, *15*(3), 1005. https://doi.org/10.3390/en15031005

Mahamood, R. M., & Akinlabi, E. T. (2017). Gas flow rate and scanning speed influence on microstructure and microhardness property of laser metal deposited titanium-alloy. In *Proceedings of the 2017 International Conference on Manufacturing and Materials Engineering* (pp. 102–108). Atlantis Press. https://doi.org/10.2991/ICMMSE-17.2017.17

Marcomini, R. F., & de Souza, D. P. F. (2011). Caracterização microestrutural de materiais cerâmicos utilizando o programa de processamento digital de imagens Image J. *Cerâmica*, *57*(341), 100–105. https://doi.org/10.1590/S0366-69132011000100013

Masoumi, M., Cardoso, J. L., de Carvalho Paes Loureiro, R., Floréz, M. A. C., Ribas, G. F., da Silva Lima, M. N., Fideles, F. F. M., Béreš, M., dos Santos, F. P., & de Abreu, H. F. G. (2025). Comparative analysis of microstructural influences on cracking in pearlitic reinforced rods steels with spheroidized vs. lamellar cementite configurations in harsh environments. *Journal of Materials Science*, *60*(43), 21436–21456.

Masoumi, M., Mohtadi-Bonab, M. A., Loureiro, R. C. P., Cardoso, J. L., Béreš, M., & Abreu,

H. F. G. de. (2024). Influence of spheroidized cementite on ferritic matrix boundary characteristics and mechanical behavior in commercial carbon steels. *Materials Research*, *27*, e20230497.

Nasiri, Z., & Mirzadeh, H. (2019). Spheroidization heat treatment and intercritical annealing of low carbon steel. *Journal of Mining and Metallurgy, Section B*, *55*(3), 405–411. https://doi.org/10.2298/JMMB180813033N

Pandit, A. S., & Bhadeshia, H. K. D. H. (2012). Divorced pearlites in steel. *Proceedings of the Royal Society A: Mathematical, Physical and Engineering Sciences*, *468*(2145), 2767–2778. https://doi.org/10.1098/RSPA.2012.0115

Pawla, V. K., Kumar, S., & Kumar, S. (2024). Enhancing resistance to corrosion, erosion and oxidation of boiler steels by surface modification techniques. *Journal of Materials and Engineering*, *2*(3), 157–169. https://doi.org/10.61552/jme.2024.03.002

Qi, M., Wu, H., Du, L., Zhang, X.-L., & Zhang, Z. (2023). Subcritical spheroidization annealing of cold-rolled Cr–Mo microalloyed medium-carbon steel with different initial microstructures. *Steel Research International*, *94*(5), 2200733. https://doi.org/10.1002/srin.202200733

Salonen, J., & Auerkari, P. (1996). *Microstructural degradation of boiler tube steels under long-term exposure to high temperature* (VTT Publications 280). VTT Technical Research Centre of Finland. ISBN 951-384938-4

Sharma, N. K., Li, L., Wang, X., Du, Y., Xu, L., & Zhao, L. (2020). Differences in service-exposed and artificially aged microstructure and tensile properties of ASTM A204 Grade C steel. *Materials Science and Technology*, *36*(18), 1967–1979. https://doi.org/10.1080/02670836.2020.1852667

Toft, L., & Marsden, R. A. (1961). *Structural processes in creep: Special report no. 70*. Iron & Steel Institute. ISBN 059862614X

Tokaji, K., Ogawa, T., & Osako, S. (1988). The growth of microstructurally small fatigue cracks in a ferritic-pearlitic steel. *Fatigue & Fracture of Engineering Materials & Structures*, *11*(5), 331–342. https://doi.org/10.1111/J.1460-2695.1988.TB01387.X

van Westen, T., & Groot, R. D. (2018). Effect of temperature cycling on Ostwald ripening. *Crystal Growth & Design*, *18*(9), 4952–4962. https://doi.org/10.1021/acs.cgd.8b00267

Vander Voort, F. G. (2000). Microindentation hardness testing. In *ASM Handbook* (Vol. 8, pp. 21–25). ASM International. https://doi.org/10.31399/ASM.HB.V08.A0003272

Wang, S., Cao, L., & Zhang, Z. (2019). Influence of carbide morphology on the deformation and fracture mechanisms of spheroidized 14CrMoR steel. *Metals*, *9*(11), 1221. https://doi.org/10.3390/met9111221

Wang, X., Du, Y., Xu, L., Zhao, L., & Han, Y. (2024). Evaluation of effect of spheroidization heat treatment on mechanical properties via small punch test. *Theoretical and Applied Fracture Mechanics*, *131*, 104353. https://doi.org/10.1016/j.tafmec.2024.104353

Yu, P., Yingjie, G., Haoran, Z., Rui, D., Guolong, Q., Haoping, P., & Lei, Y. (2025). Molecular dynamics simulation of mechanical properties of X80 steel with vacancies under different temperature and hydrogen doping. *Molecular Simulation*, *51*(6), 416–425. https://doi.org/10.1080/08927022.2025.2493940

Yu, T., Ying, C., Zhonglin, W., Gao, Z., & Zhong, F. (2024). Failure analysis of 12Cr1MoVG outlet header for the reheater of the boiler under high temperature and high-pressure environment. *Canadian Metallurgical Quarterly*, 1–11. https://doi.org/10.1080/00084433.2024.2393540

Zhao, Q.-H., Jiang, B., & Wang, J.-M. (2016). Pearlite spheroidization mechanism and lifetime prediction of 12Cr1MoV steel used in power plant. In *International Conference on Management Science and Engineering* (pp. 195–201). Atlantis Press. https://doi.org/10.2991/ICMSE-16.2016.33

Zilnyk, K. D., Suzuki, P. A., & Sandim, H. R. Z. (2023). Subtle microstructural changes during prolonged annealing of ODS-Eurofer steel. *Nuclear Materials and Energy*, *35*, 101450. https://doi.org/10.1016/j.nme.2023.101450